Earthquakes and Structures, *Vol. 9, No. 1 (2015) 49-71*
DOI: http://dx.doi.org/10.12989/eas.2015.9.1.049

Collapse response assessment of low-rise buildings with irregularities in plan

Salar Manie*[1], Abdoreza S. Moghadam[2a] and Mohsen Ghafory-Ashtiany[2b]

[1]*Department of Civil Engineering, Islamic Azad University, Sanandaj Branch, Sanandaj, Iran*
[2]*International Institute of Earthquake Engineering & Seismology (IIEES), Arghavan, North Dibajee St., Farmanieh, Tehran, Iran*

(Received November 7, 2013, Revised December 30, 2014, Accepted January 2, 2015)

Abstract. The present paper aims at evaluating damage and collapse behavior of low-rise buildings with unidirectional mass irregularities in plan (torsional buildings). In previous earthquake events, such buildings have been exposed to extensive damages and even total collapse in some cases. To investigate the performance and collapse behavior of such buildings from probabilistic points of view, three-dimensional three and six-story reinforced concrete models with unidirectional mass eccentricities ranging from 0% to 30% and designed with modern seismic design code provisions specific to intermediate ductility class were subjected to nonlinear static as well as extensive nonlinear incremental dynamic analysis (IDA) under a set of far-field real ground motions containing 21 two-component records. Performance of each model was then examined by means of calculating conventional seismic design parameters including the response reduction (R), structural overstrength (Ω) and structural ductility (μ) factors, calculation of probability distribution of maximum inter-story drift responses in two orthogonal directions and calculation collapse margin ratio (CMR) as an indicator of performance. Results demonstrate that substantial differences exist between the behavior of regular and irregular buildings in terms of lateral load capacity and collapse margin ratio. Also, results indicate that current seismic design parameters could be non-conservative for buildings with high levels of plan eccentricity and such structures do not meet the target "life safety" performance level based on safety margin against collapse. The adverse effects of plan irregularity on collapse safety of structures are more pronounced as the number of stories increases.

Keywords: torsional buildings; mass irregularities; damage; collapse; performance-based; IDA

1. Introduction

Structures with irregularities in plan, also known as torsional structures, are exposed to significant loss of strength and stiffness as compared to non-torsional counterparts under sever seismic attacks (Fardis 2009, 2010, Elnashai and Sarno 2008, Paulay 2001, Paulay and Priestley 1992). Large distance between the center of mass (CM) and center of stiffness (CR) in

*Corresponding author, Ph.D., E-mail: salarmanie@srbiau.ac.ir
[a]Associate Professor, E-mail: moghadam@iiees.ac.ir
[b]Professor, E-mail: ashtiany@iiees.ac.ir

 ISSN: 2092-7614 (Print), 2092-7622 (Online)

the linear elastic range or between the center of mass (CM) and center of strength (CV) in the nonlinear range of response are regarded as major causes of irregularity in plan. While the former case is typically considered in the seismic design of new buildings based on current seismic design codes, discussions on the latter are more found in researches. Due to the significant coupling of torsional and translational responses, performance of torsional structures is basically different from their regular counterparts. Due to the above-mentioned coupling effects, response of torsional structures is affected by various parameters and is generally accompanied by high levels of uncertainties.

In the past earthquakes, torsional structures have suffered from various structural failures and have been one of the most important causes of fatalities (Fardis 2010). In these structures which are very sensitive to higher-mode effects and rotational component of ground motion (De Stefano and Pintucchi 2008, 2002, Stathopoulos and Anagnostopoulos 2000, Paulay 2001, Wong and Tso 1994, Paulay and Priestley 1992, Hoerner 1991, Chopra 2008, Goel and Chopra 1971), distribution of seismic demands throughout the structure is non-uniform and the strength, ductility and displacement demands on the elements along the "stiff side" are generally different from such demands on the "soft side".

A key step in seismic performance evaluation of structures under sever seismic attacks is to assess their behavior in the nonlinear range of response. A comprehensive nonlinear analysis is expected to provide an estimate of the real state of the structure from the linear elastic to the highly nonlinear phases of response. In the past, extensive studies have been carried out on the nonlinear behavior assessment of reinforced concrete (RC) structures under seismic loadings to estimate the maximum demands (e.g., Fardis 2009, 2010, Elnashai and Sarno 2008, Bozorgnia and Bertero 2004). However, most of the previous studies conducted on nonlinear seismic response of torsional structures have been deterministic rather probabilistic and are generally devoted to the estimation of mean values of the peak responses (e.g., Georgoussis 2013, Marušić and Fajfar 2005, De Stefano and Pintucchi 2008, Stathopoulos and Anagnostopoulos 2000). Recognizing the variability and high degrees of uncertainty inherent in the ground motion characteristics as well as the structural elements behavior in the nonlinear range of response (especially in irregular structures), it is believed that assessing the problem from probabilistic point of view is more rational than any deterministic procedure of analysis and design.

In the past decade, evaluation of collapse behavior of structures and taking the post-peak descending branch of the structure response into consideration using nonlinear incremental dynamic analysis (IDA) and degrading nonlinear models was emerged (FEMA 2009, Zareian and Krawinkler 2007, Haselton 2006). In this regard, the document "FEMA-P695" (FEMA 2009) could be regarded as a document which offers a systematic procedure for collapse behavior assessment of structures in a probabilistic framework and contains the results of major relevant studies up to its publication. The document evaluates the safety margin against collapse (collapse-level capacity) and also provide a systematic procedure for evaluating the assumed initial seismic design parameters (such as the response modification (R), structural overstrength, (Ω) and period-based ductility (μ) factors) normally offered by modern seismic design codes. The proposed methodology in that document is probabilistic and is based on pushover analysis and nonlinear IDA results under a set of far-field and/or near-field strong ground motions. The results of such analyses are utilized for calculating the collapse margin ratio (CMR).

Collapse behavior of two-dimensional steel, reinforced concrete and wood buildings has been studied in previous publications (e.g., Goulet *et al*. 2007, FEMA P-695 2009, Haselton *et al*. 2011, Liel *et al*. 2011). Studies have also been conducted on collapse behavior of two-dimensional

frames with geometrical irregularities in elevation (Varadharajan *et al*. 2012). In contrast, less research has been devoted to the more real three-dimensional cases especially in a probabilistic framework. DeBock *et al*. (2013) studied the effects of "accidental torsion" mandated by modern seismic design codes on collapse response of three-dimensional buildings.

The present study is intended to evaluate the damage and collapse behavior of low-rise three-dimensional reinforced concrete frame buildings with uni-directional mass irregularities in plan and under the simultaneous effects of two orthogonal horizontal components of strong ground motions from a probabilistic point of view. To this end, three- and six-story RC models with uni-directional mass irregularities equal to 0% (symmetric), 10%, 20% and 30% and designed with modern seismic design codes have been subjected to nonlinear static and dynamic (incremental) analyses. For performing the IDAs, 21 normalized records selected from the far-field records set of FEMA-P695 were used. Based on the results of extensive analyses, probabilistic characteristics of the main structural response quantity (i.e., the maximum inter-story drift) were studied using probability and cumulative density functions assuming log-normal distribution of the demands. Performance of each model were also evaluated based on the post-peak and collapse responses on the basis of the procedure adopted in FEMA-P695. Finally, the seismic design factors (mentioned above) were calculated based on the recommendation of that document and compared with the initial assumed design factors. Investigation of the results reveals that by increasing the amount of mass eccentricity in plan and the number of stories, the overall performance of the structures tend to be more critical with a considerable decrease in the collapse margin ratio (CMR) as an indicator of safety margin against collapse. In some cases (typically for eccentricity values over 20%), decreases in CMR values are so pronounced that the structures could not pass the design target "life safety" performance level. Furthermore, comparison of the drifts demands and collapse margin ratios (CMRs) in symmetric and asymmetric buildings indicate significant differences.

2. Methodology

2.1. Structural models

For the evaluation process, two 3 and 6-story reinforced concrete (RC) buildings with typical structural layout as in Fig. 1(a) are considered. The models are all 3-span by 3-span moment frames designed based on ASCE/SEI 7-10 (ASCE 2010) provisions. Reinforcement detailing conform to the ACI code (ACI 2011) requirements for intermediate moment resisting frames. Span lengths are identical in both directions equal to 5 meters and story heights are considered to be 3 meters. The floor structural system is composed of one-way ribbed slabs (with parallel ribs and 5-cm concrete topping) directed in the *x*-direction of the plan (see Fig. 1). Thus the *z*-direction frames take the major portion of gravity loads. Dead and live loads on all floors are 5.3 KN/m^2 and 2 KN/m^2, respectively. All structures are assumed to be located in a very high seismicity area and the soil type is assumed to be of "firm soil" type based on ASCE/SEI 7-10 classifications. Based on the above assumptions, all of the structures belong to "SDC-D_{max}" Seismic Design Category as defined in ASCE/SEI 7-10. The concrete 28-day design (standard cylindrical specimen) and reinforcements yield strengths are selected to be 30 MPa and 400 MPa, respectively. Also, the design response modification (R) and the structural overstrength (Ω) factors are 5.00 and 3.00, respectively. These are the factors adopted in ASCE/SEI 7-10 for reinforced concrete moment frames with intermediate ductility. Figs. 1(b) and 1(c) depict the design longitudinal

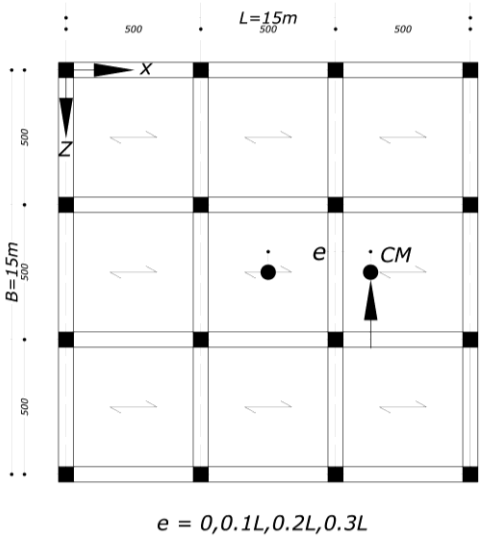

Fig. 1(a) Typical structural layout of floors

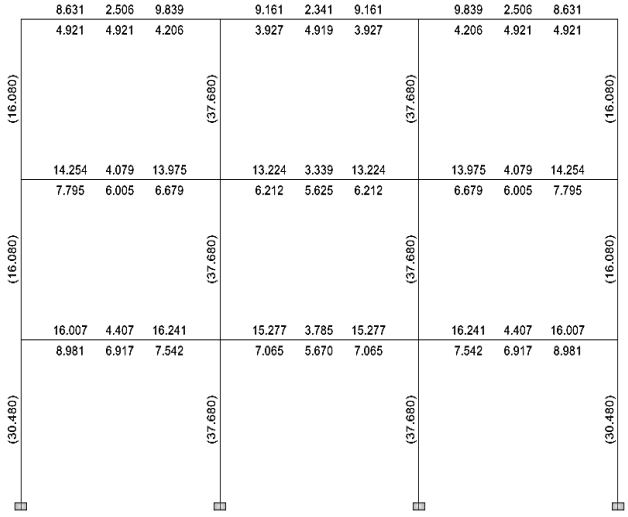

Fig. 1(b) Design longitudinal reinforcement area in a perimeter frame of the 3-story model (cm^2)

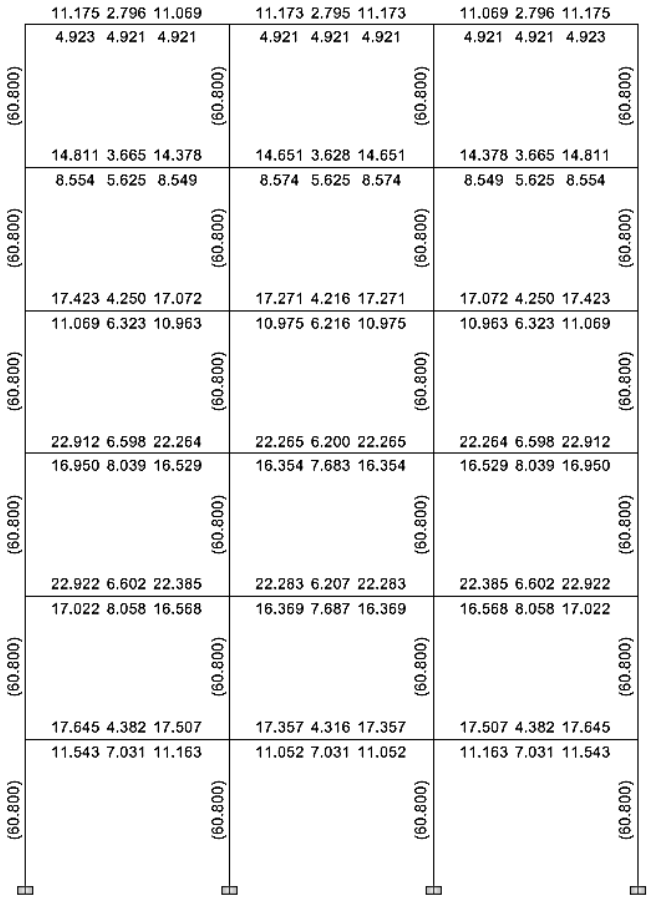

Fig. 1(c) Design longitudinal reinforcement area in a perimeter frame of the 6-story model (cm^2)

Table 1 Columns and beams sizes

3-story building	
Columns	50 cm×50 cm
x-direction beams (width×height)	35 cm×50 cm
z-direction beams (width×height)	40 cm×50 cm
6-story building	
Columns	65 cm×65 cm
x-direction beams (width×height)	45 cm×55 cm
z-direction beams (width×height)	50 cm×55 cm

reinforcements in a perimeter frame (on the soft side) of the 3 and 6-story models along the *z*-direction, respectively. Beams and columns sizes are listed in Table 1. In the analysis and design processes of all models, all lateral displacement limitations and strength requirements as mandated by ASCE/SEI 7-10 for structures of SDC-D_{max} category have been checked.

2.2 Nonlinear structural models

As discussed in Haselton (2006) and Ibarra *et al*. (2005), for collapse analysis of structures, the concentrated plasticity model (Fig. 2) is utilized in modeling with the assumption that the gravity loads are distributed uniformly on beams. This model essentially utilizes two nonlinear concentrated springs at the ends of all elements with a linear middle part which implies that the point of contra-flexure is located at mid-span of each element. In the current approach adopted for

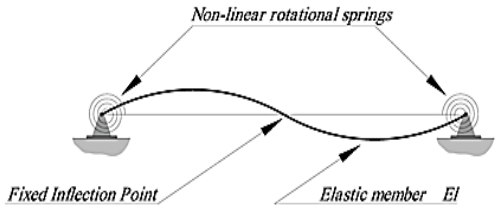

Fig. 2 Schematic representation of the concentrated plasticity model

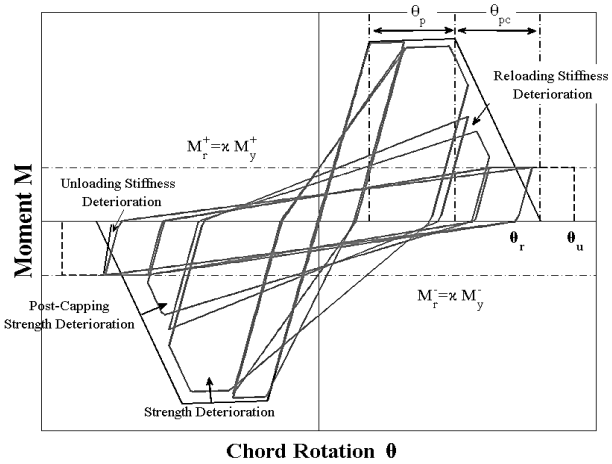

Fig. 3 Hysteretic response of RC elements with stiffness and strength degradation (Ibarra *et al*. 2005)

modeling the collapse behavior of structures (FEMA P-695 2009), all degradation effects in elements during the nonlinear phase of response including the loading and reloading stiffness, peak-strength and hardening zone stiffness degradation effects in each cycle of response could be considered in the structural properties of the springs. Based on the kinematic hardening rules, Ibarra *et al*. (2005) -based on extensive experimental tests- proposed a hysteretic model of frame elements applicable to the assessment of the nonlinear behavior of RC structures to assess their post-peak response. The model is known as "peak-oriented hysteretic model" and is depicted in Fig. 3.

Elastic analyses of all models were performed using cracked section properties. For beams, $0.35I_g$ (I_g is the gross moment of inertia of the section) and for columns, $0.70I_g$ were utilized. All the required properties of concentrated hinges including their yield rotations and yield moments, plastic and post-yield rotation capacities, energy dissipation capacity during each cycle of inelastic response, etc. have been calculated on the basis of the recommended Equations in Panagiotakos and Fardis (2001) using a graphical user interface (GUI) designed by the authors for that purpose (Manie and Moghadam 2012). As discussed in FEMA P-695, it is not required to model the beam-columns joints and bar-slip effects explicitly in the modeling process, since the available nonlinear models have been defined based on experimental tests which naturally include such effects. Geometric nonlinearities including both the global *P*-Δ and local p-delta effects were considered in the evaluation process.

Mass properties of all structures were modeled using lumped mass elements at the floor nodes. For mass eccentricity values of 10% to 30%, nodal masses at each floor were assigned in such a way that the intended plan eccentricity could be achieved. Rayleigh mass and stiffness proportional damping was considered in the nonlinear modeling process according to Zareian and Medina (2010). All models were created and analyzed in the Open Sees simulation platform (OpenSees 2011).

2.3 Analytical procedures

For the purposes of this study, all structural models were exposed to static nonlinear (pushover) as well as extensive nonlinear incremental dynamic analyses using 21 ground motions records (Vamvatsikos and Cornell 2001). Pushover analyses were performed in plan orthogonal (*x* and *z*) directions (note that in modeling, "*y*" direction is set to be upward). Since only unidirectional eccentricity perpendicular to the *z*-direction (along the *x*-direction) is considered in this study and therefore no eccentricity exists in the *x*-direction of plan, *x*-direction pushover curves are essentially identical for all models of the same height. In contrast, considerable differences are evident for the *z*-direction pushover curves (see the results section).

Plan-wise distribution of lateral load in the pushover analysis has been based on nodal mass distribution in each floor and the height-wise distribution has been based on the "first-mode" modal vectors in the desired direction as recommended in ASCE/SEI 41-06 (ASCE 2007). Control node has also been considered to be the center of mass of the roof in all structures as required by FEMA-P695 and FEMA 440 (FEMA 2005). Responses of all models have been evaluated at the center of mass, stiff and flexible sides of the plan. Details of the results will be presented in the following sections.

As mentioned, Incremental dynamic analyses were performed using a set of far-field records including 21 two-component ground motions adopted in FEMA P-695 for collapse level assessments. With the need for performing extensive nonlinear analysis, for all the analyses (with

total number of 3500 for each structure), the Multi frontal Massively Parallel Sparse Direct Solver (MUMPS) algorithm (OpenSees 2011) was utilized in three-dimensional nonlinear analysis of the models. The algorithm has been implemented in the recent versions of the Open Sees simulation platform. For all the analyses, the Newmark time-integration algorithm (Chopra 2008) was utilized. This method was very efficient in all analysis runs even at highly nonlinear stages of lateral response.

3. Results

In this section, results of pushover and IDAs are reported for the models with different plan eccentricities ranging from 0 to 30%. Results are reported using pushover curves, IDA curves along with their median curves, calculated seismic design parameters based on nonlinear static analysis results, probabilistic evaluation of spectral accelerations at the onset of collapse and performance evaluation of each model. Finally, the effects of plan eccentricity on nonlinear and collapse response of torsional buildings will be covered. Investigation of the results can provide a better insight into the collapse behavior of torsional buildings under two-component strong ground motions.

3.1 Pushover results

In this section, pushover analyses results are covered. As stated in the previous section, pushover analyses have been performed based on FEMA-P695 recommendations in both horizontal *x* and *z*-plan directions. According to FEMA-P695, the structure has to be subjected to gravity load combination of 1.05DEAD+0.25LIVE. The structures were pushed up to the state of global lateral instability (onset of collapse) or reaching a pre-assumed limit state such as shear or axial failure of elements (especially column). These limit states are termed as "non-simulated" performance criteria and need to be checked for all elements. For this purpose, one may utilize the ACI code formulas to calculate the nominal axial and/or shear capacity of beams and elements. At each stage of lateral push of the structure, if the axial and/or shear forces in any element of the structure exceed the calculated nominal strength, a "limit state" is reached and the analysis should be terminated. Non-simulated performance criteria in the form of shear failure of corner columns on the "soft-side" frames of the bottom stories were governed for both models when plan eccentricity exceeded 20% (see Figs. 4 and 5).

In Figs. 4 and 5, pushover curves are depicted for the two models in both *x* and z plan directions. Figs. 4(a) and 5(a) depict the pushover curves for the *x*-direction of 3 and 6-story models. Since no eccentricity is assumed in the *x*-direction, only one curve has been shown. As it is seen, the models were able to monitor the behavior of structures from the initial un-cracked to the highly inelastic and eventually the degrading branches of lateral response. In Figs. 4(b) and 5(b), however, significant differences are observable among the pushover curves in the *z*-direction as plan eccentricity value changes. The differences are much more pronounced in the building elastic stiffness, lateral load capacity, corresponding yield inter-story drifts and also the ultimate maximum inter-story drift values. Utilizing the data from the pushover curves, the buildings structural overstrength and period-based ductility factors are calculated according to the following equations (FEMA P-695)

$$\Omega = \frac{V_{max}}{V} \tag{1a}$$

$$\mu_T = \frac{\delta_u}{\delta_{y,eff}} \tag{1b}$$

In the above equations, $V_{\max}$ is the maximum attainable base shear of the structure, V is the code-based design base shear calculated as in Eq. (2a) below, and δ_u and $\delta_{y,eff}$ are the roof ultimate and effective yield drift values, respectively. With reference to FEMA-P695, δ_u is the roof drift corresponding to 80% of the ultimate lateral load capacity of the building (i.e., $0.8V_{\max}$). Also $\delta_{y,eff}$ can be determined either using mathematical expressions or graphical methods described in that reference.

The design base shear (V) in Eq. (1a) is calculated according to ASCE/SEI 7-10 provisions as

$$V = C_s W \tag{2a}$$

Where C_s is the seismic response coefficient calculated as in Eq. (2b) below and W is the effective seismic weight of the structure. C_s is calculated as

$$C_s = \frac{S_{DS}}{(\frac{R}{I})} \tag{2b}$$

Where S_{DS} is the design spectral response acceleration parameter in the short period range equal to 0.5 g for the assumed conditions, R is the response modification factor equal to 5 for reinforced concrete moment frames with intermediate ductility and I is the importance factor of the building equal to 1 for residential building.

Tables 2(a) to 2(d) show all the required parameters needed in Eqs. (1a) and (1b) as well as the calculated structural overstrength and period-based ductility factors for all models. All parameters are presented for the 3 and 6-sotry buildings with different mass eccentricity values, separately. In the ninth column of each table, the overstrength factor as calculated by Eq. (1a) and in the tenth column ratio of the calculated overstrength factor to the code specified value (according to ASCE/SEI 7-10) are reported for each model. In the eighth column of each table, the response

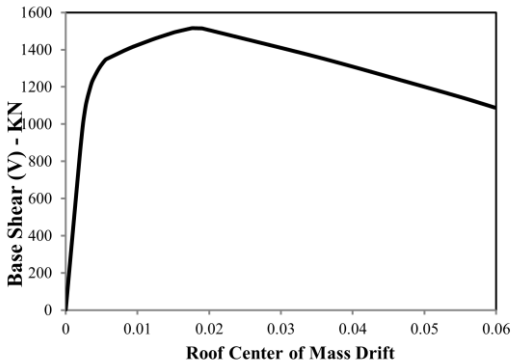

Fig. 4(a) Pushover curve for the 3-story model (*x*-direction) (Due to symmetry of response in this direction, all curves for 0 to 30% plan eccentricities are the same)

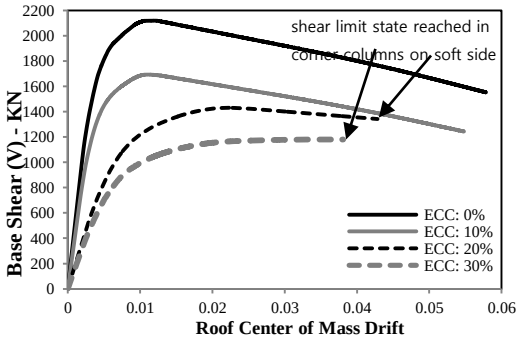

Fig. 4(b) Pushover curves for the 3-story model (*z*-direction)

modification factor (R) calculated using Eq. (3a) and (3b) are shown. For comparison, in the tenth column of the Tables, the ratio of the calculated to the code specified R-factors are also shown. In Eqs. (3a) and (3b), μ_T is the period-based ductility calculated using Eq. (2), T is the fundamental period of the structure and T_c is the transition period of design elastic spectrum between the

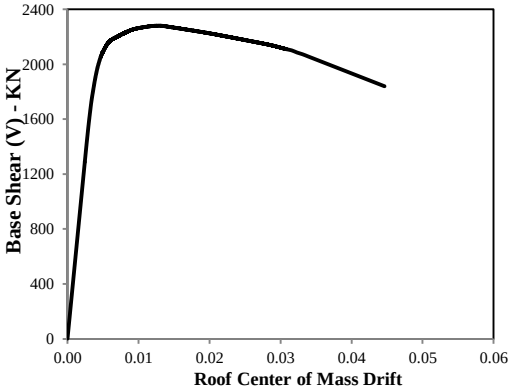

Fig. 5(a) Pushover curve for the 6-story model (x-direction) (Due to symmetry of response in this direction, all curves for 0 to 30% plan eccentricities are the same)

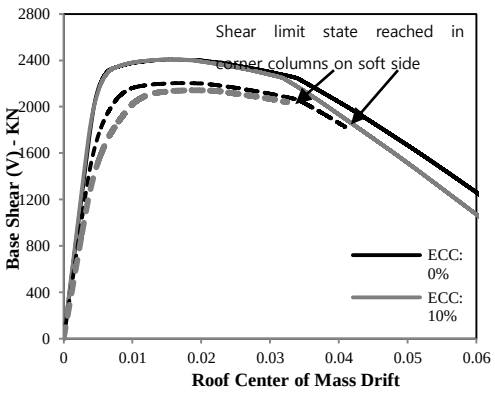

Fig. 5(b) Pushover curves for the 6-story model (z-direction)

Table 2a Pushover results for the 3-story model (x-direction)

Eccentricity (percent)	Analytical first mode period (sec.)	$V_{\max}$ (KN)	V_{design} (KN)	δ_u	$\delta_{y,eff}{}^*$	Calculated design factor			Ratio of calculated design factors to the code-specified factors	
						μ_T	R	Ω	R/R_{code}	Ω/Ω_{code}
All values	0.75	1505.55	1060.8	0.0500	0.0052	9.68	6.70	1.42	1.34	0.47

*This value has been calculated using the graphical method of FEMA-P695

(Note: due to the small differences in calculated values for all eccentricities in the x-direction, one set of values has been shown only)

Table 2b Pushover results for the 3-story model (z-direction)

Eccentricity (percent)	Analytical first mode period (sec.)	$V_{\max}$ (KN)	V_{design} (KN)	δ_u	$\delta_{y,eff}$	Calculated design factor			Ratio of calculated design factors to the code-specified factors	
						μ_T	R	Ω	R/R_{code}	Ω/Ω_{code}
ECC: 0% (Sym.)	0.69	2103.3	1060.8	0.0489	0.0052	9.37	6.50	1.98	1.30	0.66
ECC: 10%	0.81	1670.8	1060.8	0.0472	0.0062	7.61	5.34	1.58	1.07	0.53
ECC: 20%	0.84	1485.9	1060.8	0.0428	0.0076	5.63	4.04	1.40	0.81	0.47
ECC: 30%	0.93	1180.1	1060.8	0.0381	0.0088	4.32	3.18	1.11	0.64	0.37

Table 2c Pushover results for the 6-story model (*x*-direction)

Eccentricity (percent)	Analytical first mode period (sec.)	$V_{\max}$ (KN)	V_{design} (KN)	δ_u	$\delta_{y,eff}{}^*$	Calculated design factor			Ratio of calculated design factors to the code-specified factors	
						μ_T	R	Ω	R/R_{code}	Ω/Ω_{code}
All values	1.22	2285.3	1966.4	0.0460	0.0065	7.08	7.08	1.16	1.42	0.39

*This value has been calculated using the graphical method of FEMA-P695
(Note: due to the small differences in calculated values for all eccentricities in the *x*-direction, one set of values has been shown only)

Table 2d Pushover results for the 6-story model (*z*-direction)

Eccentricity (percent)	Analytical first mode period (sec.)	$V_{\max}$ (KN)	V_{design} (KN)	δ_u	$\delta_{y,eff}$	Calculated design factor			Ratio of calculated design factors to the code-specified factors	
						μ_T	R	Ω	R/R_{code}	Ω/Ω_{code}
ECC: 0% (Sym.)	1.16	2405.8	1966.4	0.0432	0.0065	6.47	6.47	1.22	1.29	0.41
ECC: 10%	1.32	2405.4	1966.4	0.0401	0.0073	5.49	5.49	1.22	1.10	0.41
ECC: 20%	1.34	2203.6	1966.4	0.0381	0.0081	4.70	4.70	1.12	0.94	0.37
ECC: 30%	1.48	2146.7	1966.4	0.0321	0.0092	3.49	3.49	1.09	0.70	0.36

constant spectral pseudo-acceleration and the constant spectral pseudo-velocity ranges. Referring to the utilized design spectrum for this study, T_c is determined to be 0.70 sec for soil type "*D*"

$$R = \mu_T \qquad if \quad T \geq T_c \tag{3a}$$

$$R = 1 + (\mu_T - 1)\frac{T}{T_C} \qquad if \quad T < T_c \tag{3b}$$

3.2 Incremental dynamic analyses results

In order to identify the damage process and also to assess the performance of structures under earthquake strong motions in terms of collapse behavior, results of incremental dynamic analyses are required (FEMA-P695 2009). This is due to the fact that nonlinear response of structures depends extensively on the characteristics of the input ground motions; i.e., the frequency content (spectral shape) and duration (FEMA-P695 2009). In essence, the collapse safety of structures needs to be assessed in a statistical and probabilistic framework under a set of incremental nonlinear time-history analyses. For this purpose, in the systematic procedure adopted in FEMA-P695, spectral intensity at the fundamental mode of the structure (in the direction of interest) on the median response spectrum of all records is scaled-up. Scaling-up continues until a global collapse state or other limit states are reached. The scaling factors (SFs) have to be computed for both horizontal directions for the desired intensity and their average is used to scale both components of each record simultaneously. This ensures consistency between both ground motion components at each level of intensity. Since three-dimensional nonlinear models have been used

for all cases, all IDAs have been performed by applying horizontal components of ground motions simultaneously.

By identifying the "collapse-level" spectral intensity of each record based on the above procedure, the collapse margin ratio (CMR) of the model can be calculated for each direction separately and their average is calculated. The average CMR is finally utilized (after some adjustments as will be discussed later) for performance assessment of the model by comparing it to the minimum acceptable values recommended in FEMA P-695 for life-safety target performance.

As pointed-out before, for conducting the IDAs, 21 normalized records selected from the "far-field" records set of FEMA-P695 were used in this study. Table 3 shows the list of the records with their PGAs. In Fig. 6, the median pseudo-acceleration spectra of both strong and weak components of all records along with the Maximum Considered Earthquake (MCE) spectrum (corresponding to exceedance probability of 2% in 50 years for the assumed conditions) are depicted. As will be discussed later, for calculating the collapse margin ratios, the "collapse-level" spectral intensities are compared against the MCE spectral intensity of the structure at its fundamental period.

Table 3 List of ground motion records used for this study

No.	**Record ID**	**Components IDs as in PEER NGA Strong Ground Motion Database (PEER 2012)**		**PGA [g]**
		Component 1	*Component 2*	
1	953	NORTHR/MUL009	NORTHR/MUL279	0.52
2	960	NORTHR/LOS000	NORTHR/LOS270	0.48
3	1602	DUZCE/BOL000	DUZCE/BOL090	0.82
4	1787	HECTOR/HEC000	HECTOR/HEC090	0.34
5	169	IMPVALL/H-DLT262	IMPVALL/H-DLT352	0.35
6	174	IMPVALL/H-E11140	IMPVALL/H-E11230	0.38
7	1111	KOBE/NIS000	KOBE/NIS090	0.51
8	1116	KOBE/SHI000	KOBE/SHI090	0.24
9	1158	KOCAELI/DZC180	KOCAELI/DZC270	0.36
10	1148	KOCAELI/ARC000	KOCAELI/ARC090	0.22
11	900	LANDERS/YER270	LANDERS/YER360	0.24
12	752	LOMAP/CAP000	LOMAP/CAP090	0.53
13	767	LOMAP/G03000	LOMAP/G03090	0.56
14	1633	MANJIL/ABBAR--L	MANJIL/ABBAR--T	0.51
15	721	SUPERST/B-ICC000	SUPERST/B-ICC090	0.36
16	725	SUPERST/B-POE270	SUPERST/B-POE270	0.45
17	829	CAPEMEND/RIO270	CAPEMEND/RIO360	0.55
18	1244	CHICHI/CHY101-E	CHICHI/CHY101-N	0.44
19	1485	CHICHI/TCU045-E	CHICHI/TCU045-N	0.51
20	68	SFERN/PEL090	SFERN/PEL180	0.21
21	125	FRIULI/A-TMZ000	FRIULI/A-TMZ270	0.35

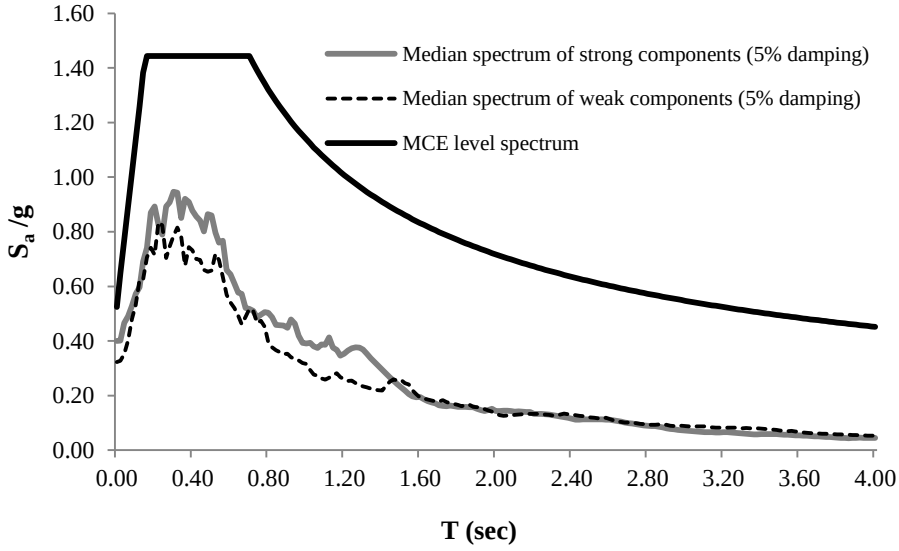

Fig. 6 Strong and weak Components median spectra of the records,and the design MCE-level spectrum

In this study three separate criteria, as below, have been used to identify the spectral intensity corresponding to the collapse state of all models along each plan direction:

1) Spectral intensity corresponding to a maximum inter-story drift value equal to 10% in the structure on the IDA curves,

2) Spectral intensity corresponding to the flattening of IDA curves,

3) Spectral intensity corresponding to reaching a specific limit state in the elements of the structure; for example, the shear and/or axial failure of columns.

The minimum spectral intensity among the values calculated based on the above (1) to (3) criteria was considered as the "collapse-level" spectral intensity (collapse capacity) of the building under the effect of each record along each plan directions.

Upon the determination of "collapse-level" spectral intensity for each record, the collapse margin ratio (CMR) can be calculated in each direction of interest based on FEMA-P695 as

$$CMR = \frac{\hat{S}_{CT}}{S_{MT}} \tag{4}$$

In Eq. (4), $\hat{S}_{CT}$ is the median of all collapse-level spectral intensities (21 values in this study) and S_{MT} is the spectral intensity at the fundamental period of vibration of the building in the direction of interest on the assumed MCE spectrum (Refer to Fig. 6 for the assumed MCE-level design spectrum). Based on the recommendations of FEMA-P695, for three-dimensional building models, the calculated CMR could be multiplied by a factor equal to 1.2 to make the analysis results consistent with two-dimensional models.

As discussed in Haselton *et al*. (2011a), Berry *et al*. (2004) and FEMA-P695 (2009), collapse capacity of structures and the calculated CMR are extensively affected by the frequency content (in other words the "spectral shape") of the ground motion records. Thus in FEMA-P695, the CMR of Eq. (4) is multiplied by a spectral shape factor (SSF) (as in Eq. (5) below) to calculate the Adjusted Collapse Margin Ratio (ACMR). ACMR is then used to assess the performance of the

Table 4 Uncertainty values selected for models considered in this study

Type of uncertainty	value
Record-to-record (β_{RTR})	0.4
Design & detailing Requirements (β_{DR})	0.2
Test data (β_{TD})	0.2
Nonlinear modeling (β_{MDL})	0.2
Total ($\beta_{Tot.}$)	**0.53**

model

$$ACMR = SSF \times CMR \tag{5}$$

In Eq. (5), SSF depends on the fundamental period as well as the period-based ductility of the model in the direction of interest. The second column of Tables 5 and 6 shows the calculated SSF based on recommendation in FEMA P-695. This factor depends on the period-based ductility and the fundamental period of vibration of the structure as well as on the seismic design category of the building based on ASCE/SEI 7-10 classification. That reference provides some tables by which one can directly estimate the SSF of the model according to the above mentioned parameters. SSF is especially important for modern buildings designed with current seismic codes in areas of high seismicity.

Another important issue in evaluating the collapse behavior of structures is the subject of "uncertainty". Uncertainty sources include those related to the ground motions, modeling, analysis, design and even construction issues (FEMA-P695 2009). Uncertainty affects the CMR directly. Low values of uncertainty are typically expected for structures with robust structural details and nonlinear models. In FEMA-P695, four sources of uncertainty related to the record-to-record (β_{RTR}), design requirements (β_{DR}), test data (β_{TD}) and nonlinear modeling (β_{MDL}) are considered in the acceptable values of CMR and other building performance criteria. Also, FEMA-P695 defines the total uncertainty as the square-root-of-sum-of-squares (SRSS) of the all uncertainty values of the above-mentioned sources. In this study, based on the recommendations of FEMA-P695 and judgment made by the authors, values as in Table 4 have been selected for the uncertainty values with the total being equal to 0.53.

Based on the acceptable 10% probability of collapse at MCE intensity level and considering "life-safety" performance target, the acceptable ACMR takes the value of 1.96 according to FEMA-P695. Thus if the calculated CMR of the model (calculated as the average of CMR for both directions as discussed earlier) becomes larger than 1.96, performance of the building is considered to be acceptable for the intended performance target, otherwise unacceptable.

Figs. 7 to 10 depict results of incremental dynamic analyses (IDAs) for the three-story models with various plan eccentricity values. Figs. 11 to 14 depict the same results for the six-story model. IDA curves (21 curves) are drawn as the spectral intensity at the fundamental mode of the structure in the direction of interest vs. the maximum inter-story drift observed in that direction for each ground motion of increasing intensity. The median curve is also shown in gray on the plots. Performance of the models is evaluated using the median curves.

Tables 5 and 6 represent the data extracted from IDA results which are central to the calculation

of the ACMRs. The results are presented for the *x*-direction and *z*-direction in the first and second rows, respectively, along with their average in the third row. The second column of each table shows the calculated spectral shape factor (SSF) of each model based on the period-based ductility factor as calculated in Table 2; the third column is the median collapse level spectral intensity ($\hat{S}_{CT}$) determined from the median IDA curve as discussed before; the fourth column is the MCE-level spectral intensity (S_{MT}) at the fundamental mode of the structure in the direction of interest; the fifth column is the calculated CMR based on Eq. (4); the sixth column is the adjusted CMR (ACMR) with the consideration of SSF factor as well as the additional 1.2 factor recommended in FEMA-P695 for three-dimensional structures, and finally the seventh column is the minimum acceptable ACMR value (equal to 1.96). By comparing the values in columns (6) and (7), performance of the structure can be regarded as "acceptable" or "unacceptable" as shown in the last column of the tables. The results will be discussed in more detail in the following sections.

Table 5 Calculation of adjusted collapse margin ratios for the 3-story model and other associated parameters

	(a) 3-story model (ECC: 0%- sym.)						
	SSF	$\hat{S}_{CT}$	S_{MT}	*CMR*	1.2×ACMR	Min. Acceptable ACMR (FEMA-P695)	Performance
Based on *X*-dir results	1.33	2.15	1.44	1.49	2.38		
Based on *Z*-dir results	1.33	2.22	1.44	1.54	2.46		
Average				1.52	2.42	1.96	Acceptable

*Based on the calculated ductility factors as in Table 2

	(b) 3-story model (ECC: 10%)						
	SSF	$\hat{S}_{CT}$	S_{MT}	*CMR*	1.2×ACMR	Min. Acceptable ACMR (FEMA-P695)	Performance
Based on *X*-dir results	1.33	1.95	1.44	1.35	2.15		
Based on *Z*-dir results	1.33	2.12	1.44	1.47	2.35		
Average				1.41	2.25	1.96	Acceptable

	(c) 3-story model (ECC: 20%)						
	SSF	$\hat{S}_{CT}$	S_{MT}	*CMR*	1.2×ACMR	Min. Acceptable ACMR (FEMA-P695)	Performance
Based on *X*-dir results	1.33	1.66	1.44	1.15	1.84		
Based on *Z*-dir results	1.29	1.69	1.44	1.17	1.81		
Average				1.16	1.83	1.96	Unacceptable

	(d) 3-story model (ECC: 30%)						
	SSF	$\hat{S}_{CT}$	S_{MT}	*CMR*	1.2×ACMR	Min. Acceptable ACMR (FEMA-P695)	Performance
Based on *X*-dir results	1.33	1.40	1.44	0.97	1.55		
Based on *Z*-dir results	1.24	1.37	1.44	0.95	1.68		
Average				0.96	1.62	1.96	Unacceptable

Table 6 Calculation of adjusted collapse margin ratios for the 6-story model and other associated parameters

	(a) 6-story model (ECC: 0%- sym.)						
	SSF	$\hat{S}_{CT}$	S_{MT}	CMR	1.2×ACMR	Min. Acceptable ACMR (FEMA-P695)	Performance
Based on *X*-dir results	1.41	1.46	1.12	1.28	2.17		
Based on *Z*-dir results	1.41	1.46	1.12	1.18	2.00		
Average				1.16	2.09	1.96	Acceptable

*Based on the calculated ductility factors as in Table 2

	(b) 6-story model (ECC: 10%)						
	SSF	$\hat{S}_{CT}$	S_{MT}	CMR	1.2×ACMR	Min. Acceptable ACMR (FEMA-P695)	Performance
Based on *X*-dir results	1.41	1.33	1.14	1.20	2.03		
Based on *Z*-dir results	1.37	1.38	1.14	1.28	2.10		
Average				1.24	2.07	1.96	Acceptable

	(c) 6-story model (ECC: 20%)						
	SSF	$\hat{S}_{CT}$	S_{MT}	*CMR*	1.2×ACMR	Min. Acceptable ACMR (FEMA-P695)	Performance
Based on *X*-dir results	1.41	1.14	1.17	1.03	1.74		
Based on *Z*-dir results	1.34	1.17	1.17	1.07	1.72		
Average				1.05	1.73	1.96	Unacceptable

	(d) 6-story model (ECC: 30%)						
	SSF	$\hat{S}_{CT}$	S_{MT}	*CMR*	1.2×ACMR	Min. Acceptable ACMR (FEMA-P695)	Performance
Based on *X*-dir results	1.41	1.00	1.17	0.85	1.43		
Based on *Z*-dir results	1.28	0.90	1.17	0.77	1.18		
Average				0.81	1.31	1.96	Unacceptable

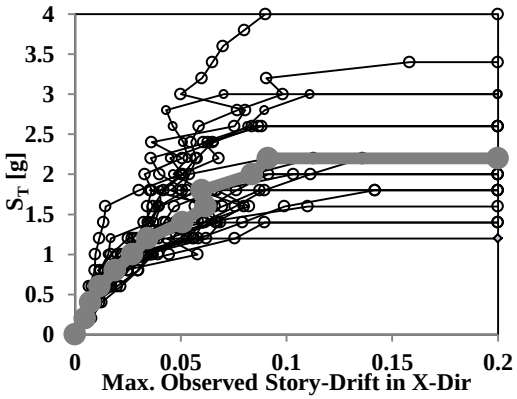

Fig. 7(a) IDA curves with the median curve (3-story model; *X*-Dir; ECC: 0%)

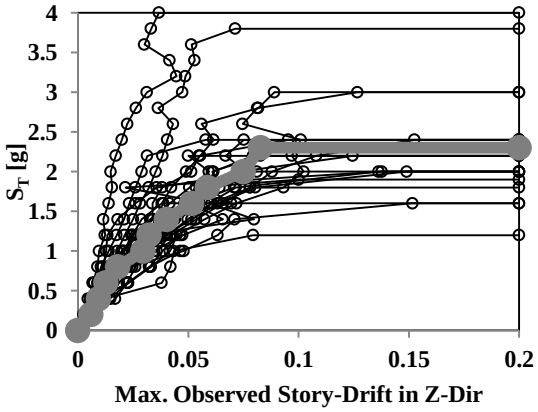

Fig. 7(b) IDA curves with the median curve (3-story model; *Z*-Dir; ECC: 0%)

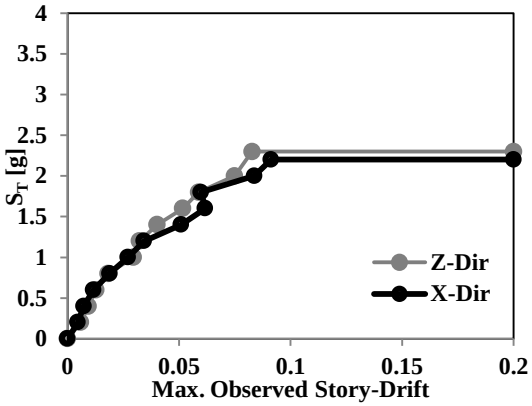

Fig. 7(c) Comparison of IDA median Curves (3-story model- ECC: 0%)

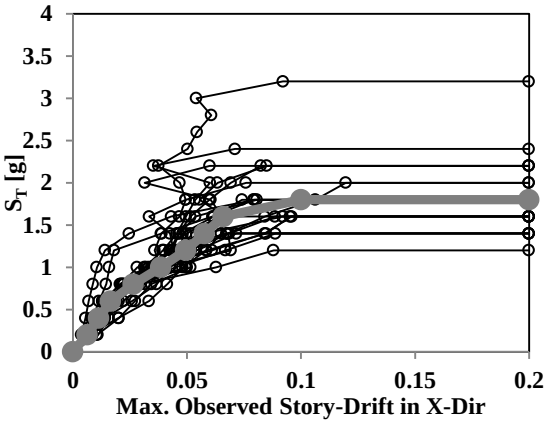

Fig. 8(a) IDA curves with the median curve (3-story model; *X*-Dir; ECC: 10%)

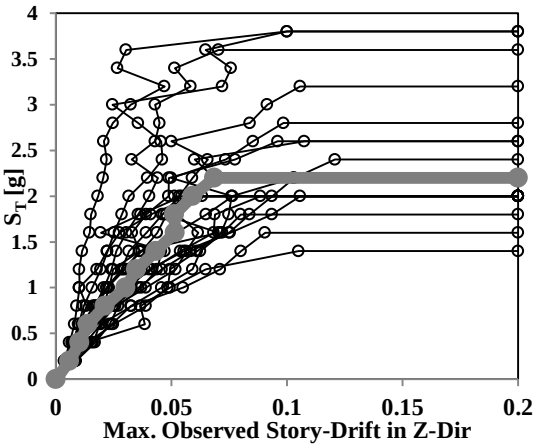

Fig. 8(b) IDA curves with the median curve (3-story model; *Z*-Dir; ECC: 10%)

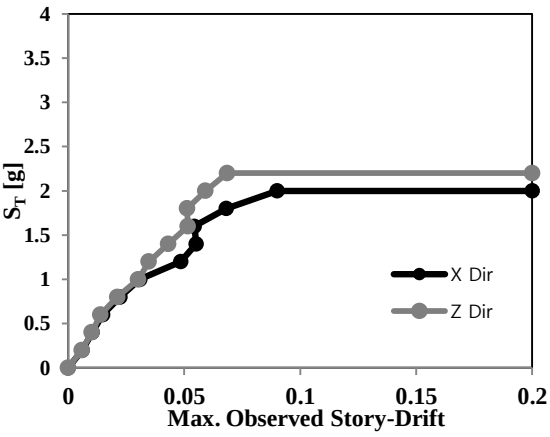

Fig. 8(c) Comparison of IDA median Curves (3-story model- ECC: 10%)

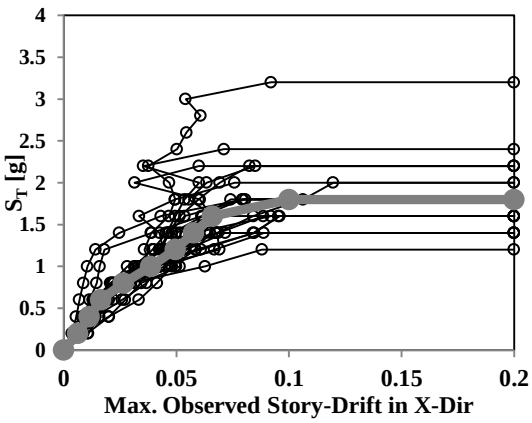

Fig. 9(a) IDA curves with the median curve (3-story model; *X*-Dir; ECC: 20%)

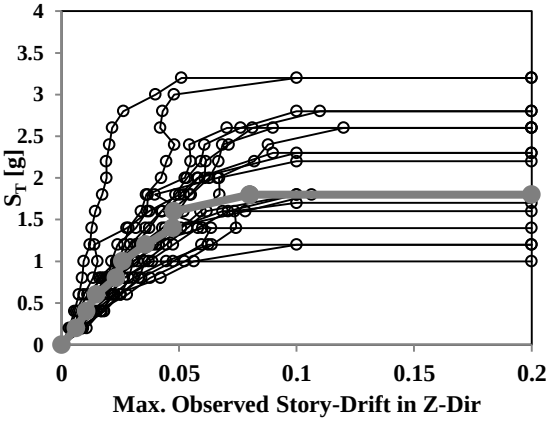

Fig. 9(b) IDA curves with the median curve (3-story model; *Z*-Dir; ECC: 20%)

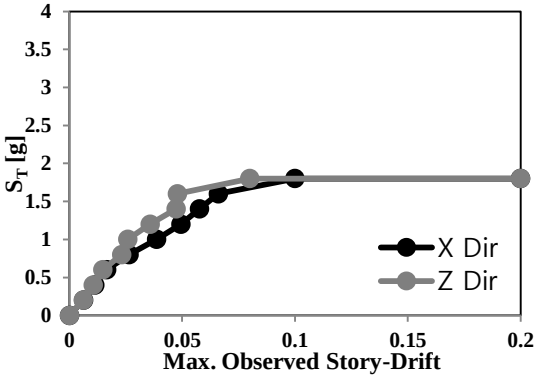

Fig. 9(c) Comparison of IDA median Curves (3-story model- ECC: 20%)

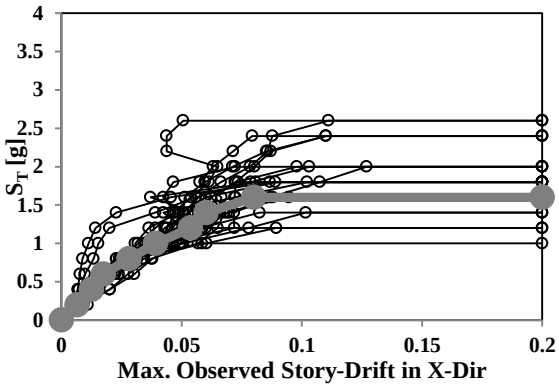

Fig. 10(a) IDA curves with the median curve (3-story model; *X*-Dir; ECC: 30%)

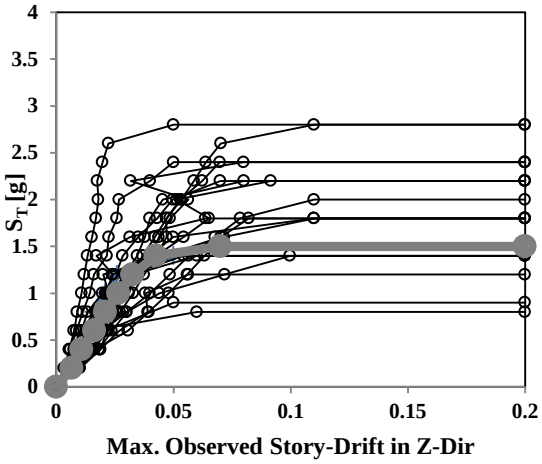

Fig. 10(b) IDA curves with the median curve (3-story model; *Z*-Dir; ECC: 30%)

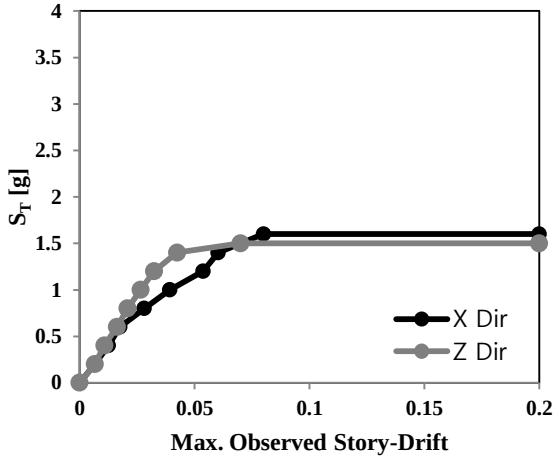

Fig. 10(c) Comparison of IDA median Curves (3-story model- ECC: 30%)

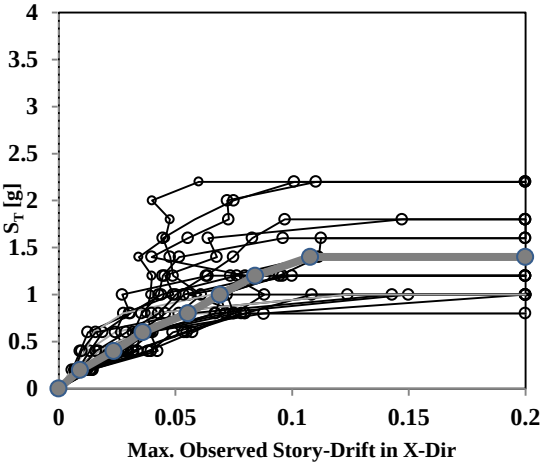

Fig. 11(a) IDA curves with the median curve (6-story model; *X*-Dir; ECC: 0%)

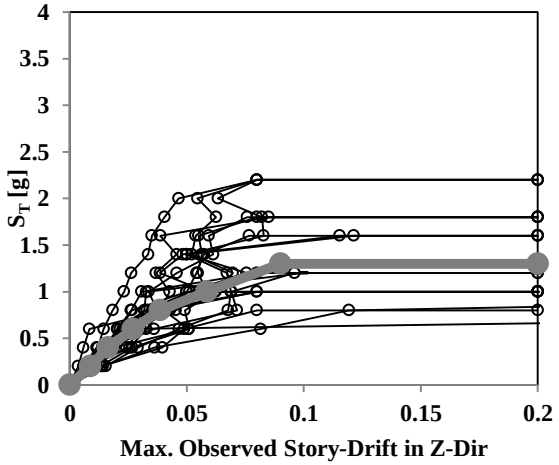

Fig. 11(b) IDA curves with the median curve (6-story model; *Z*-Dir; ECC: 0%)

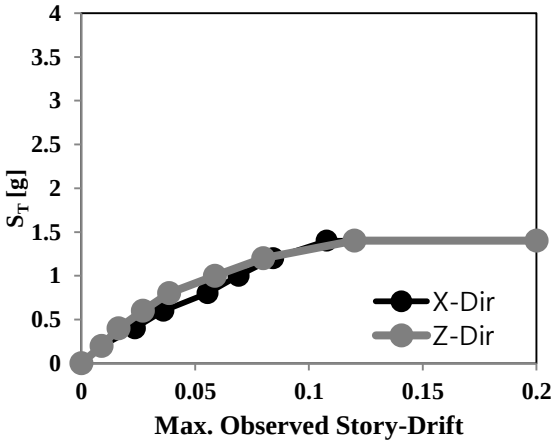

Fig. 11(c) Comparison of IDA median Curves (6-story model- ECC: 0%)

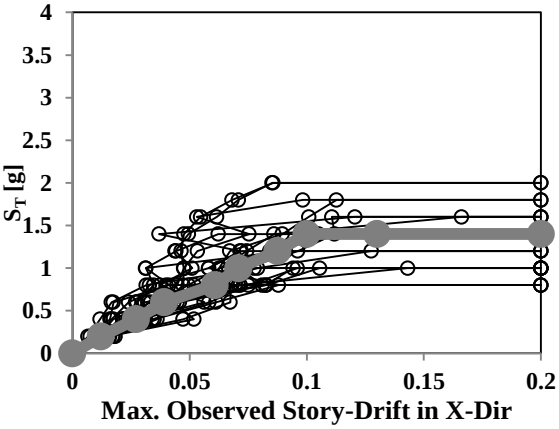

Fig. 12(a) IDA curves with the median curve (6-story model; *X*-Dir; ECC: 10%)

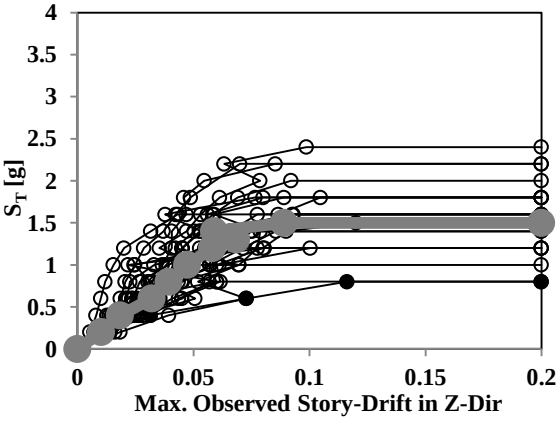

Fig. 12(b) IDA curves with the median curve (6-story model; *Z*-Dir; ECC: 10%)

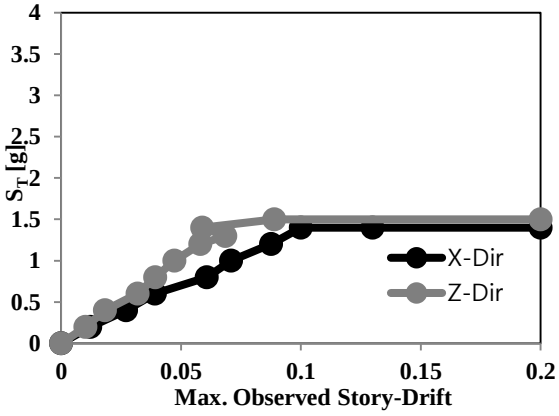

Fig. 12(c) Comparison of IDA median Curves (6-story model- ECC: 10%)

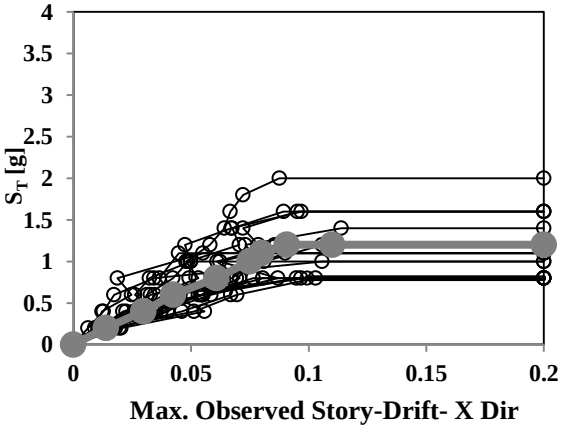

Fig. 13(a) IDA curves with the median curve (6-story model; *X*-Dir; ECC: 20%)

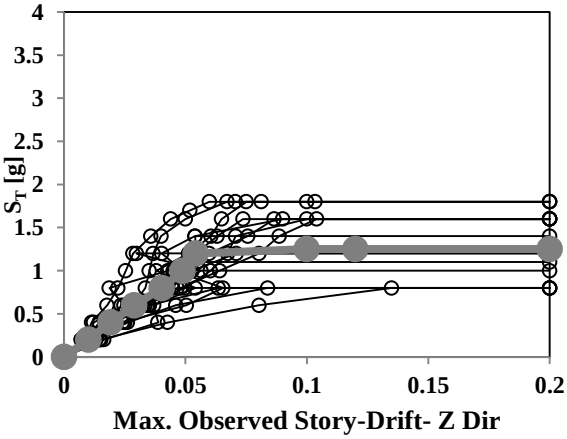

Fig. 13(b) IDA curves with the median curve (6-story model; *Z*-Dir; ECC: 20%)

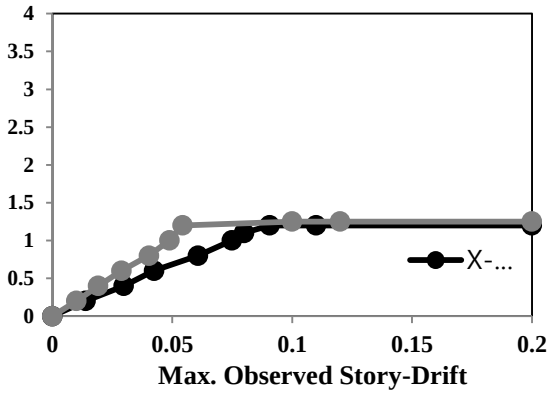

Fig. 13(c) Comparison of IDA median Curves (6-story model- ECC: 20%)

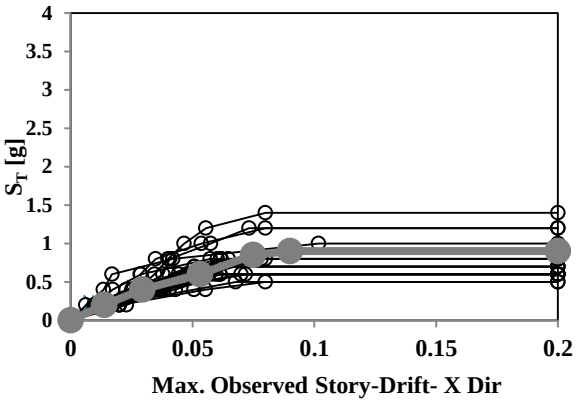

Fig. 14(a) IDA curves with the median curve (6-story model; *X*-Dir; ECC: 30%)

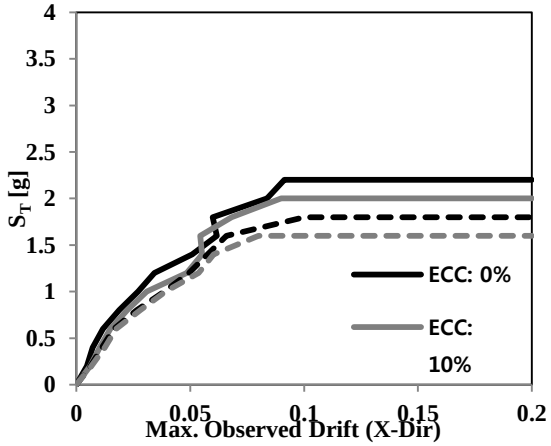

Fig. 15(a) Comparison of IDA median Curves for the 3-story model (*X*-direction)

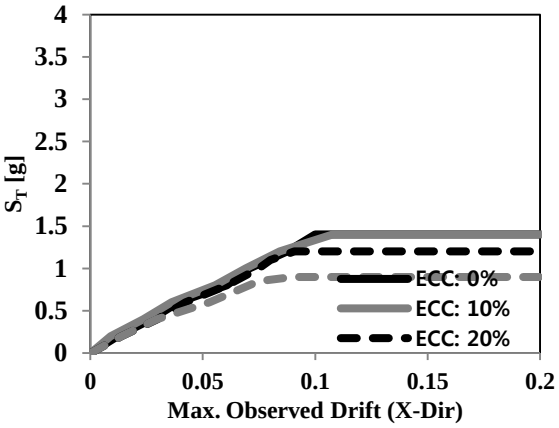

Fig. 15(b) Comparison of IDA median Curves for the 3-story model (*Z*-direction)

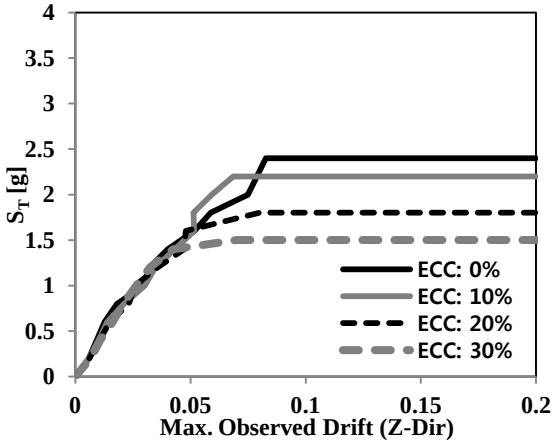

Fig. 16(a) Comparison of IDA median Curves for the 6-story model (*X*-direction)

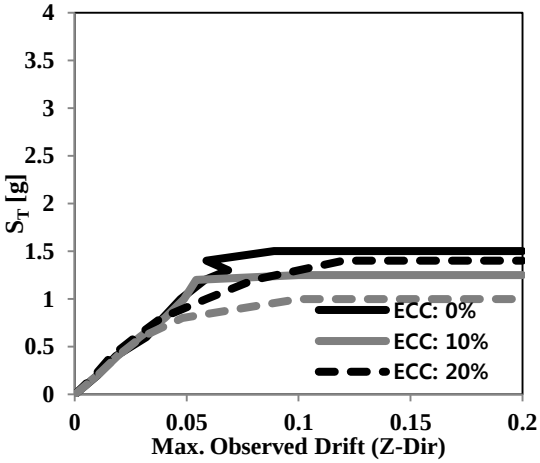

Fig. 16(b) Comparison of IDA median Curves for the 6-story model (*Z*-direction)

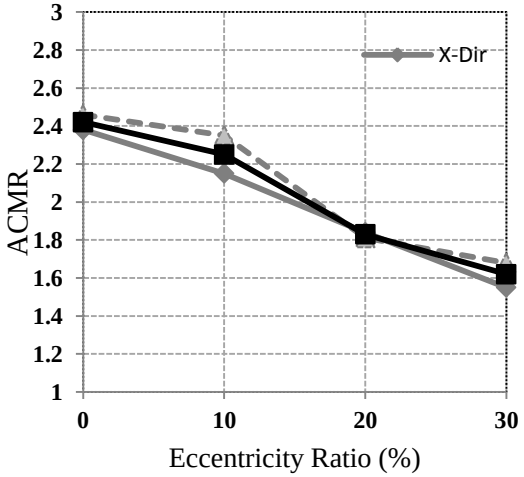

Fig. 17(a) Plan eccentricity ratio vs. ACMR (3-story model)

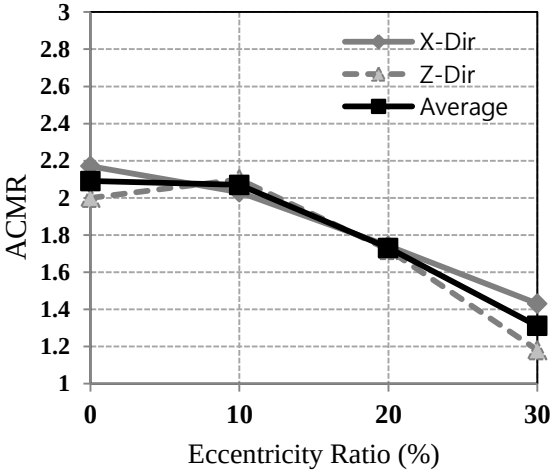

Fig. 17(b) Plan eccentricity ratio vs. ACMR (6-story model)

In Figs. 15 and 16, the median IDA curves are compared for various plan eccentricities for the 3 and 6-story models, separately. Increase in flexibility of the structure as well as significant reduction of collapse-level spectral intensities (due to the increase in the amount of plan eccentricity) are evident from these figures.

In Figs. 17(a) and 17(b), plan eccentricity ratio values are plotted against the calculated adjusted collapse margin ratio (ACMR) values for both 3 and 6-story models, respectively. In each figure, ACMRs are plotted for *x*- and *z*-directions, separately, along with their average. Reduction in the ACMR values of both directions and also in their average is evident. Examining the variation (slope) of the plotted lines shows that ACMR values reduce remarkably for structures with mass eccentricity ratios over 10%. This trend is particularly evident for the plan *z*-direction (perpendicular to the plan eccentricity) and is valid for both the 3 and 6-story buildings.

4. Discussion

Investigation of the results indicates that in low-rise buildings, by increasing the amount of plan mass eccentricity, the flexibility of the structure increases while the lateral load capacity and the maximum tolerable inter-story drift reduces. In cases of plan mass eccentricities over 10%, pushover curves show remarkable changes. Moreover, Figs. 4(b) and 5(b) confirm that for plan eccentricities over 20%, limit states, in the form of corner columns shear failure (not the global lateral instability of the buildings) become dominant in the descending region of the lateral response. In such cases, structure is exposed to premature lateral load capacity deterioration.

Examination of Tables 2(a) to 2(d) yields important aspects of nonlinear response of torsional buildings. As expected, by increasing the amount of plan mass eccentricities, the elastic vibration period of the structure in the direction perpendicular to the direction of plan eccentricity increases. From the Tables it is observed that in cases of plan mass eccentricities up to 20%, default values of response modification factors adopted in current seismic codes are generally acceptable. For

building models with plan eccentricity equal to 20% and more, however, in the direction perpendicular to the direction of eccentricity, calculated values of response modification factors are less than the default values adopted in ASCE/SEI 7-10 with the factor fall below 5.

Evaluation of the structural overstrength factors derived from the pushover analyses shows that the overstrength factor adopted in ASCE/SEI 7-10 for reinforced concrete moment frames (equals to 3) are generally conservative especially when plan irregularity increases. Furthermore, for *x*-direction frames which takes less gravity loads than the *z*-direction ones (due to the direction of gravity load transfer to these frames), the calculated overstrength factors are around 40%~50% (with some exceptions) of the factors proposed in the design code. This implies that the design overstrength factors may be different for *x*- and *z*-directions of the building even if the same structural systems have been utilized for both directions. Tables 2(b) and 2(d) also indicate that the overstrength factor reduces with increase in the amount of plan mass eccentricity values.

Comparison of the adjusted collapse margin ratios (ACMRs) in Tables 5 and 6, Figs. 15 and 16 as well as Figs. 17(a) and 17(b) shows that, generally, in all models the safety margin against collapse reduces with the increase of eccentricity in plan. The reduction is more pronounced for eccentricity values equal to 10% and more, and becomes unacceptable for eccentricity values over 20%. In these cases, reductions in the ACMR values are such remarkable that the buildings could not pass the design target "life safety" performance level according to FEMA-P695 assessment procedure based on collapse analysis of building models.

Tables 5 and 6 demonstrate that the spectral shape factor (SSF) reduces as the plan mass eccentricities increases. This phenomenon could be attributed to the reduction in period-based ductility of building models. Thus increasing the amount of plan mass eccentricities would result in reducing the spectral acceleration ($\hat{S}_c$) level corresponding to the collapse state -as mentioned previously- on one hand, and reduces the SSF, one the other; with the resultant effect being drastic reduction of ACMR. Evaluation of Figs. 15 and 16 indicates that with the increase of plan mass eccentricity, the maximum tolerable inter-story drift values corresponding to the global collapse state of the building reduce along with the reduction in collapse-level spectral intensity (collapse capacity) and increase in flexibility of the structures. Reduction in the maximum tolerable inter-story drift values at the global collapse state is very remarkable for buildings with 30% plan eccentricity.

5. Conclusions

Results of this study reveal that collapse behavior of torsional low-rise buildings designed for intermediate ductility is very different in contrast with their non-torsional counterparts designed based on current seismic design codes. Differences are observable in the calculated values of the response modification, overstrength and period-based ductility factors. Although current modern design codes such as ASCE/SEI consider less ductility capacity, and thus provide higher strength for torsionally irregular buildings in comparison to regular ones by means of special design load combinations, no specific and certain criteria are offered for direct change of the design factors according to the level of plan irregularity. Results of this study indicate that those factors need to be modified for torsional buildings based on the amount of plan eccentricity. Also, nonlinear collapse analysis results confirm that by increasing the amount of plan mass eccentricity, collapse margin ratio of the building reduces. For high levels of eccentricity values, the reduction in collapse margin ratio is so pronounced that the building does not satisfy the design target "life

safety" performance level. It seems that design codes need to address torsional effects more precisely for structures with irregularities in plan to prevent their collapse in sever seismic attacks.

Acknowledgments

The authors would like to acknowledge the anonymous reviewers for providing their valuable comments which improved the paper extensively.

References

ACI (2011), *Building Code Requirements for Structural Concrete* (ACI 318-11) *and Commentary, (ACI 318R-11)*, American concrete Institute: Farmington Hills, Michigan.

ASCE (2007), *Seismic Rehabilitation of Existing Buildings, ASCE Standard ASCE/SEI 41-06*, American Society of Civil Engineers, Reston Virginia.

ASCE (2010), *Minimum Design Loads for Buildings and Other Structures, ASCE Standard ASCE/SEI 7-05*, American Society of Civil Engineers, Reston, Virginia.

Berry, M., Parrish, M. and Eberhard, M. (2004), *PEER Structural Performance Database User's Manual.* Pacific Earthquake Engineering Research Center, University of California, Berkeley.

Bozorgnia, Y. and Bertero, V. (2004), *Earthquake Engineering: From Seismology to Performance-based Seismic Engineering*, CRS Press.

Chopra, A.K. (2008), *Dynamics of Structures: Theory and applications to earthquake engineering*, 3rd Edition, Prentice-Hall of India.

DeBock, D., Liel, A., Haselton, C.B., Hooper, J. and Henige, R. (2013), "Importance of seismic design accidental torsion requirements for building collapse capacity", *Earthq. Eng. Struct. Dyn.*, **43**(6), 831-850.

Elnashai, A.S. and Sarno, L.D. (2008), *Fundamentals of Earthquake Engineering*, John Wiley & Sons.

DeStefano, M. and Pintucchi, B. (2008), "A review of research on seismic behaviour of irregular building structures since 2002", *Bull. Earthq. Eng.*, **6**(2), 285-308.

Fardis, M.N. (2009), *Seismic design, assessment and retrofitting of concrete buildings based on EN-Eurocode 8*, Springer.

Fardis, M.N. (2010), *Advances in Performance-based Earthquake Engineering (ACES Workshop)*, Springer.

FEMA (2005), *Improvement of Nonlinear Static Seismic Analysis Procedures*, FEMA 440, Federal Emergency Management Agency, Washington, DC.

FEMA (2009), *Quantification of Building Seismic Performance Factors*, *Report No. FEMA P695*, Federal Emergency Management Agency, Washington, DC.

Georgoussis, George, K. (2013), "Yield displacement profiles of asymmetric structures for optimum torsional response", *Struct. Eng. Mech.*, **45**(2), 233-257.

Goel, R.K. and Chopra, A.K. (1971), *Inelastic seismic response of one-story asymmetric-plan systems: Effects of System parameters and yielding*, Earthquake Engineering and Engineering Research Laboratory, California Institute of Technology, Pasadena, California.

Goulet, C.A., Haselton, C.B., Mitrani-Reiser, J., Beck, J.L., Deierlein, G.G., Porter, K.A. and Stewart, J.P. (2007), "Evaluation of the seismic performance of a code-conforming reinforced-concrete frame building-From seismic hazard to collapse safety and economic losses", *Earthq. Eng. Struct. Dyn.*, **36**(13), 1973-1997.

Haselton, C.B. (2006), "Assessing seismic collapse safety of modern reinforced concrete moment-frame buildings", Ph.D. Dissertation, Department of Civil and Environmental Engineering, Stanford University, Stanford, California.

Haselton, C.B., Baker, J.W., Liel, A.B. and Deierlein, G.C. (2009), "Accounting for expected spectral shape

(epsilon) in collapse performance assessment", *Am. Soc. Struct. Eng.*, Special Publication on Ground Motion Selection and Modification.
Haselton, C.B., Baker, J.W., Liel, A.B. and Deierlein, G.G. (2011a), "Accounting for ground-motion spectral shape characteristics in structural collapse assessment through an adjustment for epsilon", *J. Struct. Eng*., **137**(3), 332-344.
Haselton, C.B., Liel, A., Deierlein, G.G., Dean, B. and Chou, J. (2011), "Seismic collapse safety of reinforced concrete buildings. I: Assessment of ductile moment frames", *J. Struct. Eng*., **137**(4), 481-491.
Hoerner, J.B. (1991), "Modal coupling and earthquake response of tall buildings. Report No. EERL 71-07", *Earthq. Eng. Struct. Dyn*., **20**(3), 201-222.
Ibarra, L.F., Medina, R.A. and Krawinkler, H. (2005), "Hysteretic models that incorporate strength and stiffness deterioration", *Int. J. Earthq. Eng. Struct. Dyn*., **34**(12), 1489-1511.
Liel, A., Haselton, C.B. and Deierlein, G.G. (2011), "Seismic collapse safety of reinforced concrete buildings. II: Comparative assessment of non-ductile and ductile moment frames", *J. Struct. Eng*., **137**(4), 492-502.
Marušić, D. and Fajfar, P. (2005), "On the inelastic seismic response of asymmetric buildings under bi-axial excitation", *Earthq. Eng. Struct. Dyn.*, **34**(8), 943-963.
Manie, S. and Moghadam, A.S. (2012), "Experiences acquired through nonlinear modeling for collapse safety assessment of 3D RC structures with irregularities in plan", *Proceedings of 15th World Conference on Earthquake Engineering*, Lisbon, Portugal.
Open Sees (2011), *Open System for Earthquake Engineering Simulation*, Pacific Earthquake Engineering research Center, University of California.
Paulay, T. and Priestley, M.J.N. (1992), *Seismic Design of Reinforced Concrete and Masonry Buildings*, John Wiley & Sons.
Paulay, T. (2001), "Some design principles relevant to torsional phenomena in ductile buildings", *J. Earthq. Eng*., **5**(3), 273-308.
Panagiotakos, T.B. and Fardis, M.N. (2001), "Deformation of reinforced concrete members at yield and ultimate", *ACI Struct. J*., **98**(2), 135-148.
Stathopoulos, K.G. and Anagnostopoulos, S.A. (2000), "Inelastic earthquake response of buildings subjected to torsion", *Proceedings of 12th World conference on earthquake engineering*, New Zealand.
Vamvatsikos, D. and Cornell, C.A. (2001), *Tracing and post-processing of IDA curves: Theory and software implementation*, Report No. RMS-44, RMS Program: Stanford University, Stanford, USA.
Varadharajan, S., Sehgal, V. and Saini, B. (2012), "Seismic response of multistory reinforced concrete frame with vertical mass and stiffness irregularities", *Struct. Des. Tall Spec. Build*., **23**(5), 362-389.
Wong, C.M. and Tso, W.K. (1994), "Inelastic seismic response of torsionally unbalanced systems designed using elastic dynamic analysis", *Earthq. Eng. Struct. Dyn*., **23**(7), 777-779.
Zareian, F. and Krawinkler, H. (2007), "Prediction of collapse-how realistic and practical is it, and what can we learn from it?", *Struct. Des. Tall Spec. Build*., **16**(5), 633-653.
Zareian, F. and Medina, R.A. (2010), "A practical method for proper modeling of structural damping in inelastic plane structural systems", *J. Comput. Struct*., **88**(1), 45-53.

CC